Global Change Biology

Global Change Biology (2013), doi: 10.1111/gcb.12193

TECHNICAL ADVANCE

Spatial relationship between climatologies and changes in global vegetation activity

ROGIER DE JONG*, MICHAEL E. SCHAEPMAN*, REINHARD FURRER†, SYTZE DE BRUIN‡ and PETER H. VERBURG§

*Remote Sensing Laboratories, University of Zurich, Winterthurerstrasse 190, 8057 Zurich, Switzerland, †Institute of Mathematics, University of Zurich, Winterthurerstrasse 190, 8057 Zurich, Switzerland, ‡Laboratory of Geo-Information Science and Remote Sensing, Wageningen University, PO Box 47, 6700AA Wageningen, The Netherlands, §Institute for Environmental Studies, VU University Amsterdam, De Boelelaan 1087, 1081HV Amsterdam, The Netherlands

Abstract

Vegetation forms a main component of the terrestrial biosphere and plays a crucial role in land-cover and climate-related studies. Activity of vegetation systems is commonly quantified using remotely sensed vegetation indices (VI). Extensive reports on temporal trends over the past decades in time series of such indices can be found in literature. However, little remains known about the processes underlying these changes at large spatial scales. In this study, we aimed at quantifying the spatial relationship between changes in potential climatic growth constraints (i.e. temperature, precipitation and incident solar radiation) and changes in vegetation activity (1982–2008). We demonstrate an additive spatial model with 0.5° resolution, consisting of a regression component representing climate-associated effects and a spatially correlated field representing the combined influence of other factors, including land-use change. Little over 50% of the spatial variance could be attributed to changes in climatologies; conspicuously, many greening trends and browning hotspots in Argentina and Australia. The nonassociated model component may contain large-scale human interventions, feedback mechanisms or natural effects, which were not captured by the climatologies. Browning hotspots in this component were especially found in subequatorial Africa. On the scale of land-cover types, strongest relationships between climatologies and vegetation activity were found in forests, including indications for browning under warming conditions (analogous to the divergence issue discussed in dendroclimatology).

Keywords: climate- and human-induced change, climatologies, Gaussian random field, growth constraints, regression, spatial additive model, vegetation-activity trends

Received 19 July 2012 and accepted 13 February 2013

Introduction

Vegetation is the main component of the terrestrial biosphere, and remotely sensed VI are commonly used in climate-change studies as a proxy for vegetation cover and photosynthetic capacity (Myneni *et al*., 1995). Changes in vegetation activity – as we use to refer to changes in vegetation index, following Zhou *et al*. (2001) – form a complex system of biotic and abiotic interactions, which differ between land-cover classes and may evolve over time themselves (Nelson *et al*., 2006). Today, VI time series are available at large spatial extents and dense time intervals. As a consequence, studying the available satellite imagery at global scale involves the analysis of large quantities of data. This has commonly been targeted with per-pixel approaches. For example, temporal VI changes have been quantified using parametric linear models on data aggregated on a yearly basis (Bai *et al*., 2008), on a seasonal basis (Eklundh & Olsson, 2003), nonparametric models on the full time series (Pouliot *et al*., 2009) or seasonal-trend decomposition algorithms (De Jong *et al*., 2012). General patterns of detected changes coincide with increasing vegetation activity over time (*greening*) in many areas of the world, conspicuously in Europe (Stöckli & Vidale, 2004; Julien *et al*., 2006), the Sahel (Eklundh & Olsson, 2003; Anyamba & Tucker, 2005; Herrmann *et al*., 2005; Hickler *et al*., 2005; Olsson *et al*., 2005), India (Jeyaseelan *et al*., 2007) and the Northern Hemisphere in general (Tucker *et al*., 2001; Zhou *et al*., 2001; Slayback *et al*., 2003). Decreases (*browning*), on the other hand, have been identified in parts of the Southern Hemisphere (e.g. South America), but also in boreal forests (De Jong *et al*., 2012). These results illustrate the temporal change in vegetation activity over the past decades, but leave relationships with underlying processes open. Relationships with climate, including oceanic oscillations (Woodward *et al*., 2008), can be anticipated and have been substantiated by various modelling (Nemani *et al*.,

Correspondence: Rogier de Jong, tel. +41446355162, fax +41446356846, e-mail: rogier.dejong@geo.uzh.ch

2003; Zhao & Running, 2010) and correlation (Kawabata *et al.*, 2001; Ichii *et al.*, 2002; Xiao & Moody, 2005) studies. Apart from climatic drivers, changes may be induced by anthropogenic processes such as land-use change, or by a combination of both (Evans & Geerken, 2004). For these reasons, disentangling all contributing drivers at large spatial scales remains an unsolved issue (Xiao & Moody, 2005). Typical spatial resolutions ranging from 0.05 to 0.5° complicate the issue as they always involve mixed pixels, consisting of several vegetation types and other land-use/land-cover types (Alcantara *et al.*, 2012; Van Asselen & Verburg, 2012).

Climate observations (temperature, precipitation, cloudiness, among others) are available globally as gridded data sets with monthly intervals since the beginning of the previous century (Mitchell & Jones, 2005). At the same time, variations in vegetation activity have been inferred from satellite imagery at global scale since the early 1980s (Tucker *et al.*, 2005) using the normalized difference vegetation index (NDVI). This index directly correlates with the fraction of absorbed photosynthetically active radiation (fPAR) and can – in combination with an efficiency conversion factor and the amount of incident PAR – be used to quantify gross primary productivity (Running *et al.*, 2004). Using these data sources, associations between climate change and changes in vegetation activity can be made for the last decades (Fensholt *et al.*, 2012). Such associations are likely to vary with land cover, as each class may respond differently to climate change and to land-use change (Chapin *et al.*, 2000; Verburg *et al.*, 2011).

In this study, we modelled the observed changes in vegetation activity as the additive combination of fixed (climate-associated) effects, spatially dependent random effects and independent residuals. We developed a land-cover–specific deterministic model and a globally applicable regression-tree approach to associate variation in vegetation activity with climate changes. Covariates for these models were selected under the assumption that maximum plant growth is affected by either one or any combination of three climatological constraints: water availability, temperature and incident radiation (Field *et al.*, 1995). This assumption was found to hold for most parts of the terrestrial surface (Churkina & Running, 1998). Other environmental control factors are not accounted for in this model. These may include changes in hydrology (e.g. permafrost thaw), atmospheric characteristics (e.g. wind, humidity, biological and chemical constituents), species composition, degradation of soil (nutrient) resources or land use and management. The effects of these factors on vegetation activity were expected to be spatially autocorrelated (Zhou *et al.*, 2001). Therefore, we tested the application of a spatially autocorrelated Gausian random field (GRF) model for representing the combined effect of all other drivers not accounted for in the climatology-driven model.

Accordingly, in this work, we hypothesized that a part of the spatial variation in vegetation-activity trends can be associated with trends in potential growth-limiting climatologies. This research investigated this hypothesis by quantifying the role of trends in climatologies on vegetation activity as well as the associated geographical distribution. Furthermore, realizing that the system of causation is complex, we aimed at quantifying the combined response of nonmodelled drivers (including land-use change), in terms of length scale and strength, as a spatial field. We demonstrate that the maps associated with this decomposition reveal spatial patterns that help the interpretation of relationships between vegetation activity, climate change and human-induced changes.

Materials and methods

Data

NDVI record. The National Oceanographic and Atmospheric Administration (NOAA) acquired the longest series of data using advanced very high-resolution radiometer (AVHRR) sensors. We used the latest release of the global inventory modelling and mapping studies (GIMMS) NDVI*g* data set, which is an extension of earlier versions (Tucker *et al.*, 2005). The data set consists of 28 years (from 1981 through 2008) of fortnightly acquisitions at ~8 km (0.072°) spatial resolution. The fortnightly scenes are maximum value composites of daily 4 km global area coverage data. This procedure largely removes atmospheric noise (Holben, 1986), although some inaccuracy remains, especially in hazy and cloudy conditions (Nagol *et al.*, 2009). We applied the harmonic analysis of NDVI time series (HANTS) interpolation algorithm (Roerink *et al.*, 2000; De Jong *et al.*, 2011) to remove remaining noise in areas with persistent cloud cover. Areas with very sparse or no vegetation cover (yearly median NDVI < 0.1) were masked out, as well as regions at higher than 72° northern latitude. As such, we excluded the northernmost regions of Russia and Canada where NDVI signals have been found impacted by high solar zenith angles and by snow and ice (Brown *et al.*, 2006). Orbital decay and changes in NOAA satellites are known to affect AVHRR data, but processed NDVI data have been found free of trends introduced from these effects (Kaufmann *et al.*, 2000). Alcaraz-Segura *et al.* (2010), Baldi *et al.* (2008) and Zhou *et al.* (2001), among others, provided discussions on the quality of GIMMS and derived trends.

Climate data. The Climatic Research Unit (CRU: University of East Anglia Climatic Research Unit, 2008) provides high-resolution gridded data sets with global coverage. The latest TS 3.1 data sets (Mitchell & Jones, 2005) were released in April 2011 and updated in July 2012 because of a systematic error in the precipitation data. The data sets provide time series for a range of climate parameters (Table 1). In the CRU processing

Table 1 Climate parameters from the CRU TS 3.1 data set (Mitchell & Jones, 2005). Each parameter is represented in a high-resolution monthly grid with a spatial resolution of 0.5°, for the time span 1901–2009. PET (monthly mean mm day^{-1}) was multiplied by the number of days in each month to obtain mm month^{-1}. PRE was taken from the recent CRU TS 3.10.1 data set

Label	Parameter	Unit
CLD	Cloud cover	%
DTR	Diurnal temperature range	°C
FRS	Frost day frequency	days
PRE	Precipitation	mm
TMP	Daily mean temperature	°C
TMN	Daily minimum temperature	°C
TMX	Daily maximum temperature	°C
VAP	Vapour pressure	hPa
WET	Wet day frequency	days
PET	Potential evapotranspiration	mm

scheme, several station-based data sources were harmonized to obtain most reliable estimates. For each parameter, reference climatologies (or: normals) were calculated for the 1961–1990 period and deviations from the normal (or: anomalies) were calculated for all measurements in the record. After spatial interpolation and superposition on the reference climatologies, these anomalies constitute the final 0.5° grids (720 × 360 cells). See Mitchell & Jones (2005) for details about the data sources and processing steps. The data sets cover 1901–2009 and subsets matching the time span of GIMMS were used here. Nonterrestrial pixels were masked, resulting in approximately 65 000 grid cells per corresponding GIMMS time step.

Climatologies were selected under the assumption that plant growth is limited by water availability, temperature and/or incident radiation (Field *et al*., 1995). Changes in either of these parameters might induce changes in vegetation productivity and in the proxy NDVI signal. For most regions, water availability is determined by the amount of precipitation, although snow melt should be taken into account in high northern latitudes and in mountainous regions. In this study, we confined this parameter to precipitation as productivity in the mentioned regions is temperature limited rather than water limited (Nemani *et al*., 2003). Time series of incident PAR are not globally available, but the amount of PAR is to a large extent determined by the intensity and duration of cloud overcast (Zhuravleva *et al*., 2006). Furthermore, the CRU cloud-cover data have been augmented with PAR-related sunshine records to complement sparse cloud observations in recent decades (Mitchell & Jones, 2005). For these reasons, trends in temperature (TMP), precipitation and cloud cover (CLD) were selected as covariates for the deterministic prediction of NDVI trends. Potential Evapotranspiration (PET) is a reflection of the energy available to evaporate water given that ample water is available. It may reflect growth limitation by radiation and was adopted as additional covariate. PET was calculated as reference value for grass according to the method used by the United Nations Food and Agricultural Organization (Ekström *et al*., 2007), which is a variant of the Penman-Monteith method (Allen *et al*., 1994). The gridded TMP, TMN, TMX, VAP and CLD (Table 1) were used as input for this calculation. PET units are mm day^{-1} and were multiplied by the number of days in each month to obtain mm month^{-1}.

Land-cover data. In the International Geosphere and Biosphere Programme (IGBP), a 1 km land-cover product (DISCover) was developed. The data set consists of 17 general land-cover types (Loveland & Belward, 1997; Loveland *et al*., 2000), based on AVHRR data and a vegetation-classification logic that is climate independent (Running *et al*., 1994). The classification scheme was later adopted within the moderate-resolution imaging spectrometer (MODIS) land-cover products (Friedl *et al*., 2002). We used the 2009 MCD12C1.005 product, which provides aggregated land cover at 0.05° resolution, as well as the subpixel frequency of each class. The product is based on a full year of composited 8 days MODIS observations (reflectance and land-surface temperature) and can be considered representative for the state of the land surface around the end of our analysis period. This information was used to develop land-cover–specific regression models. Figure 1 provides a conceptual design of the various processing steps that are discussed in the following sections.

Spatial aggregation of NDVI and land-cover data. The native spatial resolution of the CRU TS 3.1 climate data is 0.5°, whereas the land-cover data from the MCD12C1 product and the GIMMS NDVI data have spatial resolutions of 0.05° (~5.6 km) and 0.073° (~8 km) respectively. Therefore, both the land-cover data and the temporal NDVI trends needed to be resampled to 0.5° spatial resolution. In case of the discrete land-cover data, the spatial aggregation scheme affects the prevalence of the different classes and the spatial coherence of each land-cover class within the aggregated product (Dendoncker *et al*., 2008; Verburg *et al*., 2011). For this reason, careful selection of the aggregation scheme is crucial. A central pixel approach best preserves the relative area of the individual classes, especially the minor classes. A majority approach, on the other hand, provides the best result in terms of spatial structure of the major classes. In this study, we adopted the

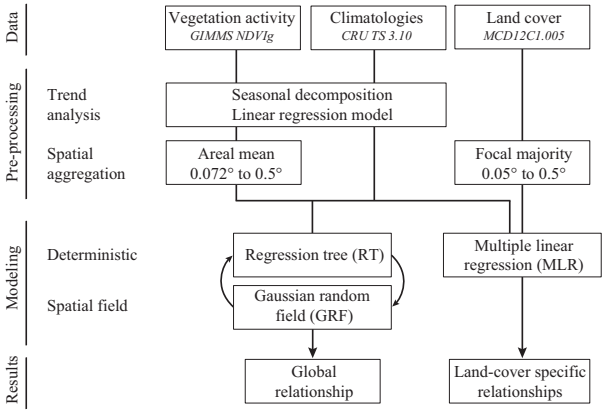

Fig. 1 Conceptual design of the various data sources and processing steps.

majority scheme to assign the prevailing land-cover class (Fig. 2a) and we used the subpixel frequency (Fig. 2b) to select relatively homogeneous pixels for fitting the regression models. The original GIMMS data were used for determination of temporal trends in NDVI between 1982 and 2008 at 0.073° (~8 km) spatial resolution. The resulting map of vegetation-activity changes was aggregated to 0.5° using the areal mean. All analyses were carried out using R statistical software (R Development Core Team, 2012) and the geospatial data abstraction library (GDAL, 2012).

Temporal changes in vegetation activity and climatologies

The total amount of change was determined for both NDVI and climate time series using linear regression after seasonal adjustment (De Jong *et al.*, 2011). The seasonality was modelled by using additive harmonic functions with periods of 12, 6 and 3 months respectively. The seasonal component was subtracted from the original data before fitting the linear model. The magnitude of change was obtained by multiplying the slope coefficient of the fitted model by the length of the time series. As mentioned before, trend analysis was applied before any spatial resampling was performed. The resulting change maps (Fig. 3) were used for the additive model, which is described in the next section. Significance of the slope coefficients was assessed using generalized least squares. In this way, possible short-lag temporal autocorrelation, which remains after subtracting the seasonal component, is accounted for in the calculation of the *P*-values. All trends at 0.05 confidence level were

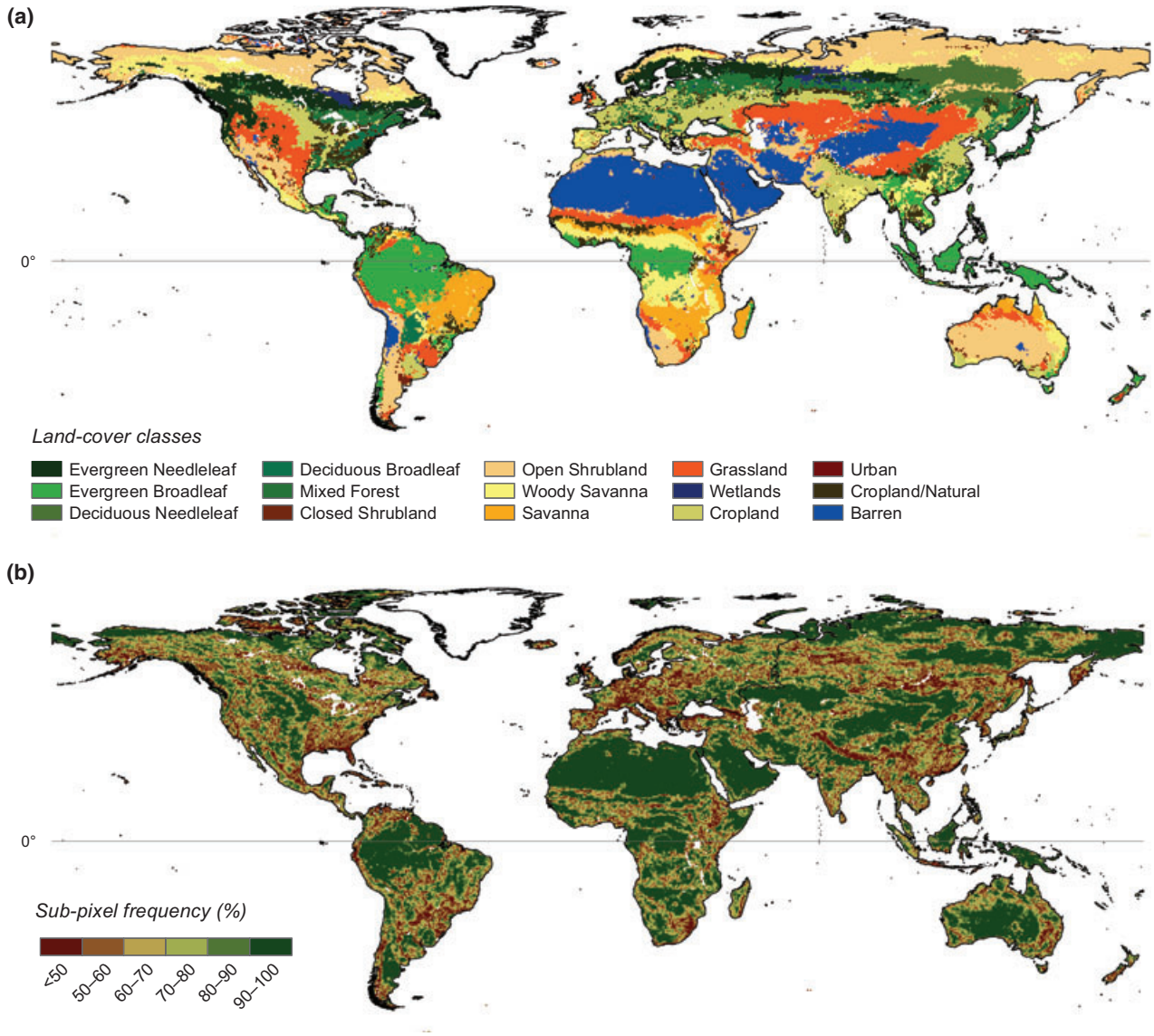

Fig. 2 (a) Major land-cover classes derived from the 2009 moderate-resolution imaging spectrometer MCD12C1 product and the International Geosphere-Biosphere Programme classification scheme (Loveland *et al.*, 2000). The data were resampled to 0.5° spatial resolution using a majority resampling approach. (b) Subpixel frequency of the major land-cover classes (%).

retained; other slope coefficients were neglected (and appear as zero values in Fig. 3).

Based on the climatologies, two regression approaches – one land-cover specific [multiple linear regression (MLR)] and one globally applicable [regression tree (RT)] – were used.

Land-cover–specific model for observed NDVI changes

Different land-cover classes (or biomes) are likely to respond differently to changes in climatic conditions (Chapin *et al.*, 2000). To assess the relative influence of each of the four climatologies, we used land-cover–specific MLR models. Eqn 1 shows the common structure for each of the 12 models. In this equation, β_n represents regression coefficients and the climatologies vector [Δ_n] contains changes in the CRU parameters (Table 1) as covariates. The latter were determined for the same time span as the NDVI data using seasonal decomposition and a linear trend model. For the seasonal decomposition, we estimated the seasonal signal using the HANTS algorithm (Roerink *et al.*, 2000; De Jong *et al.*, 2011). The model (i.e. β) was parameterized for each of the 12 land-cover classes separately.

$$\Delta\mathrm{NDVI} = \beta_0 + \begin{bmatrix} \Delta\mathrm{TMP} \\ \Delta\mathrm{PRE} \\ \Delta\mathrm{CLD} \\ \Delta\mathrm{PET} \end{bmatrix}^{\mathrm{T}} \times [\beta_1\ \beta_4]^{\mathrm{T}} + \varepsilon \qquad (1)$$

At 0.5° spatial resolution, land cover is in most cases a composite of smaller patches, whereas homogeneous pixels are needed for model calibration. The subpixel frequency (Fig. 2b) of each class was used to exclude heterogeneous pixels for calibrating the regression models described in Eqn 1. The highest homogeneity threshold (i.e. the fraction of the 0.5° cell covered by a unique class) was selected such that the individual land-cover classes retained sufficient pixels for calibration. Above 80%, the number of grid cells in smaller land-cover classes (deciduous broadleaf forest and closed shrubland) appeared too limiting for model training and (bootstrapped) significance tests. At the 80% level, permanent wetlands – the major land-cover class in 514 grid cells (<1%) – was the only vegetated land-cover class that could not be incorporated into the model.

Clusters of pixels in large, homogeneous regions (e.g. Siberia, Amazon and the Great Plains) cause spatial dependency in the training data. While estimating model coefficients, a bootstrapping method was applied to avoid spatial-autocorrelation effects. This provides the possibility to calculate confidence intervals for the regression coefficients and to exclude covariates with an insignificant deviation from zero ($\alpha = 0.05$). The maximum number of bootstrap samples was set to 1000 for each land-cover class.

Global model for observed NDVI changes

An additive model was used for describing the observed temporal changes in NDVI (observations y). The model consists of a deterministic part where y depends on a set of covariates x with their coefficients β (fixed effects), a spatial process h and a residual white noise component ε (Eqn 2).

$$y = x^{\mathrm{T}}\beta + h + \varepsilon \qquad (2)$$

The individual components were estimated using a backfitting approach, consisting of an iterative estimation of the fixed effects β (regression step) and the spatial field h (kriging step). The procedure is stepwise described as follows.

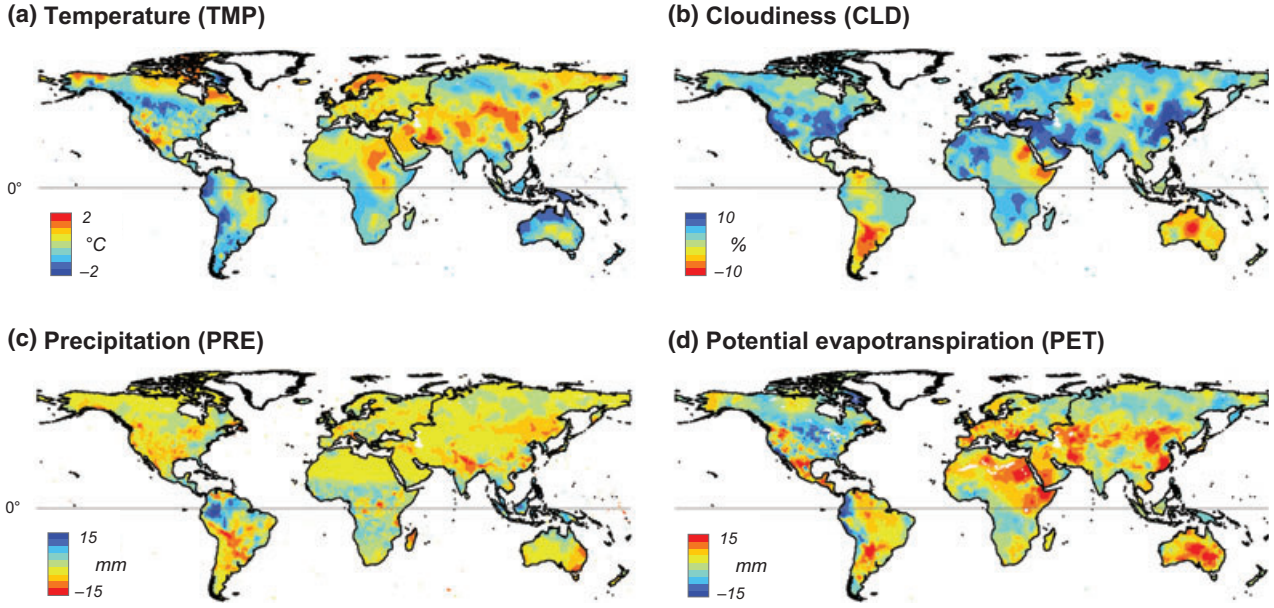

Fig. 3 Temporal changes (1982–2008) in climatologies: (a) temperature, (b)cloudiness, (c) precipitation (PRE) and (d)potential evapotranspiration. Changes were derived at 0.5° spatial resolution using linear models, after seasonal decomposition, from monthly gridded data [Climatic Research Unit (CRU) time series (TS) 3.1/CRU TS 3.10.1 for PRE] (Mitchell & Jones, 2005).

(step 1): The initial fixed-effect component $x^T\beta$ was estimated using a RT model.

(step 2): The initial spatial $\hat{h}^{(0)}$ field was fitted using the residuals of step 1 by the method of moments for prediction of the spatial field parameters. This method is affected by both the random variation and the variation represented by the fixed effects (Lark *et al.*, 2006); the backfitting approach in the next step pursues optimal parameter estimation in this situation of mutual model dependency.

(step 3): The initial spatial field was subtracted from the observations and the fixed effects were re-estimated (step 1). These were, in turn, subtracted from the observations to predict h (step 2) and this iteration was continued until convergence. Formally, convergence cannot be proved (Furrer & Sain, 2009), but empirically it was found that the parameter estimation stabilized after a few iterations.

The deterministic model (step 1) and the spatial field (step 2) are described briefly in the following sections and in more detail in the supporting online material (SMO).

Deterministic model (fixed effects)

The IGBP land-cover classification is climate independent and each class combines geographically spread regions (e.g. Siberian tundra and African thickets) in summary classes such as 'open shrubland'. To deal with these and other interactions, a flexible RT approach was chosen instead of an application of a global MLR model. An RT is a sequence of binary splits of the full data set (independent of land-cover class), each time using the explanatory variable (i.e. one of the climatologies) that produces the most homogeneous branches according to a least squares criterion (see Section S1 for a more elaborate description). The downside of this approach is the limited transparency of the predictor importance. Several methods can be used to estimate variable importance, but their robustness is debated and its measures are not straightforward (Steinberg, 2009). To profit from both, we followed the approach as described in Section 2.4 allowing to get insight in the relative importance of the explanatory variables (i.e. climatologies) in specific land-cover regions and the RT approach at global scale.

Spatial field model (random effects)

The regression-tree model is a per-pixel approach, which does not account for spatial dependence, other than induced by the explanatory variables. Spatial dependence can be imposed by modelling h as a stationary GRF. This component quantifies how much of the variation (beyond climate effects) is spatially correlated, that is can be explained by yet unknown underlying spatial processes. The GRF is described by a mean function (here constant zero), a range parameter δ that determines the length scale of the spatial dependency and a sill that determines the marginal variance. A spherical function was used to model the reduction in covariance with increasing distance up to the maximum distance δ, beyond which the spatial dependency was forced to zero. The optimal range was found to be around 900 km and was fixed before optimizing the sill parameter using maximum likelihood estimation. The estimated parameter set was used to model the spatial field h. The model is further described in Section S2.

Residual component

An almost pure-nugget variogram (not shown) indicated that the pixel values in the residual component are spatially uncorrelated. This implies that the combination of fixed and random effects captured virtually all spatial variance at 0.5° resolution. As mentioned before, the within-pixel variation due to smaller scale processes (<0.5°) remains unexplained.

Results and discussion

Model predictions

Land-cover–specific associations. Bootstrapped regression models provided insight in land-cover–specific associations between vegetation-activity and growth-limiting climate parameters. The performance, in terms of coefficient of determination (R^2), varied among land-cover classes (Table 2). There appeared to be a difference between forest and nonforest areas especially. The strongest relationships were found in forests, with the highest R^2 in deciduous classes and the lowest R^2 in the (tropical) evergreen broadleaf class. The latter was anticipated for several reasons: the use of NDVI is disputed in tropical regions (Huete *et al.*, 1997), climatological observations are relatively sparse (Zhao & Running, 2011) and vegetation growth may not (only) be limited by the climatologies used (Churkina & Running, 1998). Outside of forests, the strongest relationship was found for closed shrubland (e.g. parts of the Sahel region) whereas the weakest relationship was found for open shrubland. The likely explanation of the latter is a heterogeneous distribution of this land-cover class over the globe (Fig. 2a). It includes, among other regions, the tundra, large parts of the African bush lands and thickets, central Australia and Argentina, each of which can be expected to react differently to climate changes (Chapin *et al.*, 2000, chapter 2). For such reasons and as discussed before, the regression-tree approach was adopted for global prediction.

Table 2 suggests that the relationship between cloudiness, which was used as proxy for incident radiation, and vegetation activity is more conspicuous for nonforest than for forest classes. A positive relationship between cloudiness and vegetation activity was found for all classes but savanna, which suggests that a reduction in incident radiation yields a positive impact on vegetation

Table 2 Results of the bootstrapped multiple regression model. For each of the nonmasked land-cover classes following Loveland *et al*., (2000), the table lists the coefficient of determination of the fitted model (R^2) and the Pearson correlation coefficient between the change in normalized difference vegetation index and the parameters used in the model. Homogeneous grid cells (subpixel frequency > 80%) were used for model training and climate parameters that did not significantly ($\alpha = 0.05$) contribute to the model were not included

			Correlation coefficient			
	Land-cover class	R^2	TMP	PRE	CLD	PET
Forest	Evergreen needleleaf	0.43	0.65			0.25
	Evergreen broadleaf	0.22		0.17		−0.16
	Deciduous needleleaf	0.54	−0.57	−0.26		−0.32
	Deciduous broadleaf	0.68	−0.23		0.79	
	Mixed	0.25	0.14			−0.14
Nonforest	Closed shrubland	0.59		0.67	0.17	0.36
	Open shrubland	0.08	0.12		0.25	−0.17
	Woody savanna	0.20	0.38		−0.37	0.32
	Savanna	0.10	0.16	0.06	−0.12	0.10
	Grassland	0.22		0.14	0.30	−0.20
	Cropland	0.13	0.07		0.28	
	Cropland/natural mosaic	0.20			0.30	

TMP, temperature; PRE, precipitation; CLD, cloud cover; PET, potential evapotranspiration.

activity in, among others, grasslands and croplands. A candidate explanation of this might be found in the higher influence of the diffuse component of incoming PAR, as compared with the direct component (Spitters *et al*., 1986). Clouds were adopted as a proxy for incident PAR, but they do not act as on/off switch for incident radiation. Rather, they determine the ratio between direct and diffuse radiation. For this reason, the efficiency of photosynthesis under overcast skies may be underestimated (Roderick *et al*., 2001; Gu *et al*., 2002). For some land-cover systems, the combination of higher temperatures and reduced cloudiness may increase the potential evapotranspiration, but limit vegetation activity, indications for which could be seen for savannas. These ecosystems are predominantly water limited, rather than temperature limited (Nemani *et al*., 2003), for which an increase in PET may not reflect in higher activity of canopies. The observed cloudiness associations may also be related to changes in global radiative forcing. A reduction, or global *dimming*, has been suggested for the 1960s until late 1980s, but it was suggested that the trend inversed towards global *brightening* afterwards (Wild *et al*., 2005). The latter was found to have raised the diffuse fraction of solar radiation, which, in turn, may have boosted photosynthetic efficiency.

Vegetation activity in the (boreal) needleleaf classes shows associations with temperature – as anticipated (Nemani *et al*., 2003) – although the deciduous needleleaf forests (Russia) show reduced vegetation activity despite the warming trend (Fig. 3; Table 2). This case of boreal browning has been referred to as the *divergence problem* and underlying processes remain largely unknown (D'Arrigo *et al*., 2008). Suggested causes include drought stress, pollution, global dimming, direct temperature stress and, likely, a combination of these (Goetz *et al*., 2011). Drought stress would be consistent with field observations in relatively dense forests (Goetz *et al*., 2011) and radiation-related causes may be expected in other cases, although in this study only found through association with potential evapotranspiration. Radiation–hydrology feedback mechanisms may further complicate this issue (Oliveira *et al*., 2011; Girardin *et al*., 2012). Finally, increased biomass burning (Soja *et al*., 2004) might have contributed to feedback mechanisms not fully covered within this approach.

Global associations with climatologies. Figure 4 shows the decomposition of the changes in vegetation activity into the fields described by the fixed effects (RT), the spatial process (GRF) and the uncorrelated residuals. The prediction based on the optimal regression-tree model fit (in terms of lowest cross-validation error) explained 54% of the spatial variation and is shown in the second panel of Fig. 4.

The general pattern of changes in vegetation activity is well captured by the fixed-effects model (i.e. by the changes in climatologies), although the greening patterns seem better represented than some of the browning patterns (e.g. in subequatorial Africa). A strong association between greening and precipitation was found in closed shrublands (Table 2), including parts of the Sahel. This region is known for its long anomalously dry period since the early 1970s (Nicholson, 2000), probably related to multidecadal oceanic

oscillations (Zhang & Delworth, 2006). The record-low years were just before the satellite recordings and since then a positive trend in both precipitation and vegetation activity was found (Fensholt & Rasmussen, 2011), which likely underlies the detected association (Hickler *et al.*, 2005). Nevertheless, associations were found to vary at regional scales (Bégué *et al.*, 2011; Hein *et al.*, 2011) and remaining greening and browning patches were therefore found in the GRF component.

Nonassociated spatial patterns. Large-scale browning patterns appeared in the spatially correlated field, which implies that they could not be directly associated with climate change. The underlying processes, however, are likely to act at large spatial scales. Here, we discuss some conspicuous regions including an effort to identify candidate drivers from literature.

In Africa, two regions stand out: south/east of Lake Victoria (mainly Tanzania) and Zimbabwe/southern Mozambique. In the former, the changes might be partly related to human activities, as the fixed-effect model indicated small increases in vegetation activity rather than decreases. In recent decades, population increased and agriculture intensified accordingly. Although small parts of the area are in protected national parks (e.g. Serengeti), the browning hotspots are concentrated in unprotected woodland and grassland, parts of which were previously marked as degraded (Pelkey *et al.*, 2000). Wind erosion and overgrazing have been mentioned as causes for degradation in these regions (Dregne, 2002).

Severe degradation was also found in Zimbabwe and attributed to human land use, concentrated in communal areas (Prince *et al.*, 2009). While relating potential productivity to actual productivity in this region, Prince *et al.* (2009) could establish no relationship between productivity declines and climatic factors, which is consistent with our results. In South Africa, similar conclusions were drawn based on NDVI analysis with correction for changes in precipitation (Wessels *et al.*, 2007). Despite this, it remains contentious to assign browning patterns to land degradation, partly because its definition includes perception aspects and because the NDVI signal needs to vary substantially to capture the complex interaction of drivers (Wessels *et al.*, 2012).

Browning in Indonesia and other places of south-east Asia might be related to the expansion of rubber and palm oil plantations at the cost of tropical forest, a conversion that has been documented to take place at scales large enough to be visible as browning in the analysis (Mann, 2009; Koh *et al.*, 2011). Other conspicuous browning regions include large parts of the needleleaf forests in Alaska, Canada and Russia. For these regions, the complicated relationship with climate and other abiotic factors was discussed in the previous section.

The random-effects component also revealed greening patterns that might be associated with land-use processes. Very obvious is the large-scale greening in Eastern Europe and the former Soviet Union. This greening is documented in the literature as being related to land abandonment in the postsocialist period, leading to large-scale regrowth of natural vegetation (Baumann *et al.*, 2011; Alcantara *et al.*, 2012; Prishchepov *et al.*, 2012).

The Sahel region showed patches of spatially correlated greening and browning. This indicates that – although the overall greening of the region can be reasonably associated with climate effects – large interregional deviations exist. This can be explained by the complex interactions between land use, grazing and climate that exist in this region (Seaquist *et al.*, 2008; Bégué *et al.*, 2011; Hein *et al.*, 2011). These complex interactions cause spatial and temporal deviations in the greening impact of a wetter climate and therefore lead to the patchy pattern.

Remainder

The remainder component in Fig. 4d is spatially uncorrelated (variogram not shown). This component may contain small-scale human interventions, indirect climate effects – likely hidden in feedback mechanisms uncaptured at the given spatiotemporal scale – or measurement error (Zhou *et al.*, 2001). It should, however, be noted that a substantial part of the local variation caused by small-scale processes was averaged out in the spatial aggregation procedure. Climatological observations at higher spatial resolution would be needed to further disentangle these processes.

Limitations and outlook

The results from the presented model showed plausible associations between limiting climate variables and vegetation activity. However, the approach also contains limitations that may guide future research. First of all, it is important to stress that correlation, on which this study relied, does not mean causation. The presented statistical methods form no physical process model and there are many processes that cannot be resolved while being of influence at the spatial scale the model was applied. For example, the large browning effect in Northern Argentina (mainly the Chaco region) was largely attributed to the climatologies (Fig. 4b). This area, however, is also known for large-scale land conversion into arable farming (Viglizzo *et al.*, 2011). As both could be responsible for the browning effect,

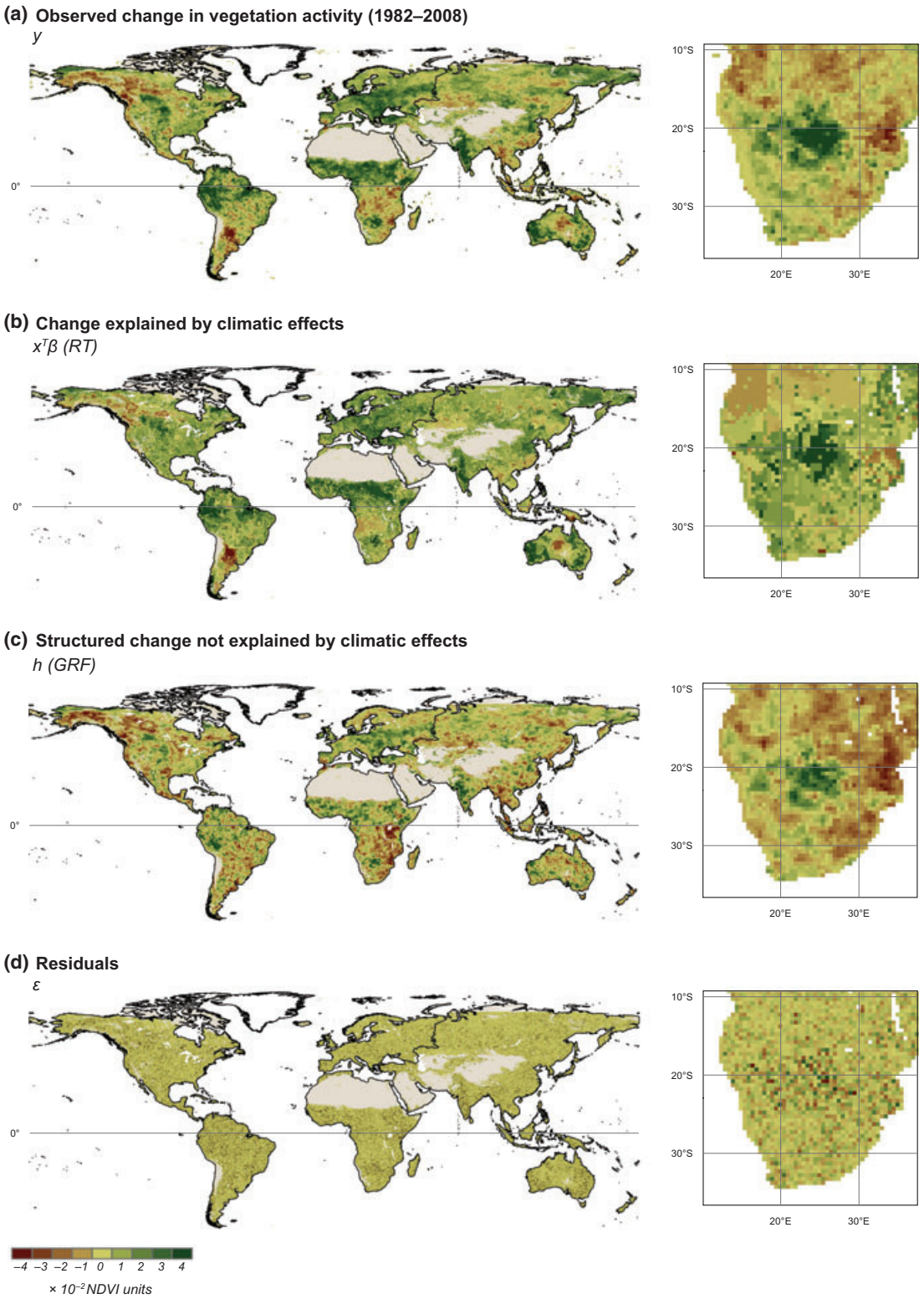

Fig. 4 Decomposition of (a) the observed changes in vegetation activity into (b) fixed climatology effects as represented by the regression-tree model, (c) other spatially correlated, or 'structured', effects as represented by the Gaussian random field and (d) residual term ε. The four insets illustrate the spatial structure of each model component at pixel level for the example of southern Africa. For few grid cells, fixed effects could not be estimated and, as a result, the spatial field was not predicted, due to masking of water bodies and permanent wetlands (e.g. Lake Malawi in the insets).

 Global Change Biology, doi: 10.1111/gcb.12193

the causation and correct partitioning of the effects is difficult to establish (Zak *et al.*, 2008). Sophisticated modelling of the deterministic component, including mentioned climate–vegetation feedback mechanisms, might be achieved with full spatial-temporal models, but comes with challenges. For example, estimation of many model parameters, given only NDVI as response variable, is likely to run into an ill-posed scenario. Furthermore, dynamic temporal lags between some climatic predictors and vegetation response need to be accounted for. The latter is neither simple nor straightforward at large spatial and temporal extents (Eklundh, 1998; Bégué *et al.*, 2011).

The predictive power of the gridded climate data at hand is reduced by the spatial interpolation, that is the effective number of observations is lower than the number of 0.5° grid cells. This might inflate the weight of the current GRF component. A denser climate observation network would increase the predictive power, especially in remote areas, although great value of the CRU data set resides in its time span. As regards the cloudiness data, the observations have been augmented with sunshine records (Mitchell & Jones, 2005) and few observations are available outside of Europe, North America and Asia. Both may bias the prediction and render radiation the component where improvement is most needed.

Conclusions

In this study we hypothesized that a part of the spatial variation in vegetation-activity changes can be attributed to changes in potential growth-limiting climatologies (i.e. temperature, precipitation and radiation proxies) and that the remainder shows spatial patterns, which can be used to quantify the combined influence of other actors, including human effects. By modelling the deterministic climate effects and the nonassociated spatial process, we found the following:

1. At global scale, the deterministic relationship with climatologies explained about 54% of the spatial variation in vegetation-activity trends. In geographical sense, it especially accounted for large parts of the global greening trends and for the browning hotspots in Argentina and Australia.
2. The spatially correlated field, which combines actors other than climatologies, explained the majority of the remaining variation, leaving a minimal share in the residual component. For some sub-Saharan regions, including Tanzania and Zimbabwe, browning hotspots were detected within this component. In these regions, negative changes in vegetation activity may need to be explained by human activities. Other hotspots could be related to well-documented large-scale land conversions.
3. Land-cover–specific regression models demonstrated strongest relationships between climate change and vegetation-activity trends in forests, conspicuously in needleleaf forest. Here, negative relationships with temperature showed reduced vegetation activity under warming conditions: an effect, which is known as the divergence problem in boreal forests. Strong positive relationships between precipitation and vegetation activity were found in closed shrublands.

Acknowledgements

We are grateful to Molly Brown and the GIMMS group for providing their data set and to Rama Nemani for sharing the source data of Fig. 2a in Nemani *et al.* (2003). We are grateful for excellent reviewer comments. We acknowledge support of the UZH Research Priority Program (URPP) on 'Global Change and Biodiversity'. Authors sequence is listed following the SDC approach (doi: 10.1371/journal.pbio.0050018).

References

Alcantara C, Kuemmerle T, Prishchepov AV, Radeloff VC (2012) Mapping abandoned agriculture with multi-temporal MODIS satellite data. *Remote Sensing of Environment*, **124**, 334–347.

Alcaraz-Segura D, Chuvieco E, Epstein HE, Kasischke ES, Trishchenko A (2010) Debating the greening vs. browning of the North American boreal forest: differences between satellite datasets. *Global Change Biology*, **16**, 760–770.

Allen R, Smith M, Perrier A, Pereira L (1994) An update for the definition of reference evapotranspiration. *ICID Bulletin*, **43**, 1–34.

Anyamba A, Tucker CJ (2005) Analysis of Sahelian vegetation dynamics using NOAA-AVHRR NDVI data from 1981–2003. *Journal of Arid Environments*, **63**, 596–614.

Bai ZG, Dent DL, Olsson L, Schaepman ME (2008) Proxy global assessment of land degradation. *Soil Use and Management*, **24**, 223–234.

Baldi G, Nosetto M, Aragón R, Aversa F, Paruelo J, Jobbágy E (2008) Long-term satellite NDVI data sets: evaluating their ability to detect ecosystem functional changes in South America. *Sensors*, **8**, 5397–5425.

Baumann M, Kuemmerle T, Elbakidze M *et al.* (2011) Patterns and drivers of post-socialist farmland abandonment in Western Ukraine. *Land Use Policy*, **28**, 552–562.

Bégué A, Vintrou E, Ruelland D, Claden M, Dessay N (2011) Can a 25-year trend in Soudano-Sahelian vegetation dynamics be interpreted in terms of land use change? A remote sensing approach. *Global Environmental Change*, **21**, 413–420.

Brown ME, Pinzon JE, Didan K, Morisette JT, Tucker CJ (2006) Evaluation of the consistency of long-term NDVI time series derived from AVHRR, SPOT-vegetation, SeaWiFS, MODIS, and Landsat ETM+ sensors. *IEEE Transactions on Geoscience and Remote Sensing*, **44**, 1787–1793.

Chapin FS, Zavaleta ES, Eviner VT *et al.* (2000) Consequences of changing biodiversity. *Nature*, **405**, 234–242.

Churkina G, Running SW (1998) Contrasting climatic controls on the estimated productivity of global terrestrial biomes. *Ecosystems*, **1**, 206–215.

CRU: University of East Anglia Climatic Research Unit (2008) Jones, Phil and Harris, Ian (investigators): CRU Time Series (TS) high resolution gridded datasets. NCAS British Atmospheric Data Centre. Available at: http://badc.nerc.ac.uk/view/badc.nerc.ac.uk__ATOM__dataent_1256223773328276 (accessed 8 July 2011).

D'Arrigo R, Wilson R, Liepert B, Cherubini P (2008) On the 'Divergence Problem' in Northern Forests: a review of the tree-ring evidence and possible causes. *Global and Planetary Change*, **60**, 289–305.

De Jong R, De Bruin S, De Wit A, Schaepman ME, Dent DL (2011) Analysis of monotonic greening and browning trends from global NDVI time-series. *Remote Sensing of Environment*, **115**, 692–702.

De Jong R, Verbesselt J, Schaepman ME, De Bruin S (2012) Trend changes in global greening and browning: contribution of short-term trends to longer-term change. *Global Change Biology*, **18**, 642–655.

Dendoncker N, Schmit C, Rounsevell M (2008) Exploring spatial data uncertainties in land-use change scenarios. *International Journal of Geographical Information Science*, **22**, 1013–1030.

Dregne HE (2002) Land degradation in the drylands. *Arid Land Research Management*, **16**, 99–132.

Eklundh L (1998) Estimating relations between AVHRR NDVI and rainfall in East Africa at 10-day and monthly time scales. *International Journal of Remote Sensing*, **19**, 563–570.

Eklundh L, Olsson L (2003) Vegetation index trends for the African Sahel 1982–1999. *Geophysical Research Letters*, **30**, 1430.

Ekström M, Jones PD, Fowler HJ, Lenderink G, Buishand TA, Conway D (2007) Regional climate model data used within the SWURVE project, 1: projected changes in seasonal patterns and estimation of PET. *Hydrology and Earth System Sciences*, **11**, 1069–1083.

Evans J, Geerken R (2004) Discrimination between climate and human-induced dryland degradation. *Journal of Arid Environments*, **57**, 535–554.

Fensholt R, Rasmussen K (2011) Analysis of trends in the Sahelian 'rain-use efficiency' using GIMMS NDVI, RFE and GPCP rainfall data. *Remote Sensing of Environment*, **115**, 438–451.

Fensholt R, Langanke T, Rasmussen K *et al.* (2012) Greenness in semi-arid areas across the globe 1981–2007 – an Earth Observing Satellite based analysis of trends and drivers. *Remote Sensing of Environment*, **121**, 144–158.

Field CB, Randerson JT, Malmström CM (1995) Global net primary production: combining ecology and remote sensing. *Remote Sensing of Environment*, **51**, 74–88.

Friedl MA, Mciver DK, Hodges JCF *et al.* (2002) Global land cover mapping from MODIS: algorithms and early results. *Remote Sensing of Environment*, **83**, 287–302.

Furrer R, Sain SR (2009) Spatial model fitting for large datasets with applications to climate and microarray problems. *Statistics and Computing*, **19**, 113–128.

GDAL (2012) GDAL – Geospatial Data Abstraction Library, Open Source Geospatial Foundation. Available at: http://gdal.osgeo.org (accessed 10 August 2011).

Girardin MP, Guo XJ, Bernier PY, Raulier F, Gauthier S (2012) Changes in growth of pristine boreal North American forests from 1950 to 2005 driven by landscape demographics and species traits. *Biogeosciences Discuss*, **9**, 1021–1053.

Goetz SJ, Epstein HE, Bhatt US *et al.* (2011) Recent changes in arctic vegetation: satellite observations and simulation model predictions. In: *Eurasian Arctic Land Cover and Land Use in a Changing Climate* (eds Gutman G, Reissell A), pp. 9–36. Springer-Verlag, Amsterdam.

Gu L, Baldocchi D, Verma SB, Black TA, Vesala T, Falge EM, Dowty PR (2002) Advantages of diffuse radiation for terrestrial ecosystem productivity. *Journal of Geophysical Research*, **107**, 4050.

Hein L, De Ridder N, Hiernaux P, Leemans R, De Wit A, Schaepman ME (2011) Desertification in the Sahel: towards better accounting for ecosystem dynamics in the interpretation of remote sensing images. *Journal of Arid Environments*, **75**, 1164–1172.

Herrmann SM, Anyamba A, Tucker CJ (2005) Recent trends in vegetation dynamics in the African Sahel and their relationship to climate. *Global Environmental Change Part A*, **15**, 394–404.

Hickler T, Eklundh L, Seaquist JW *et al.* (2005) Precipitation controls Sahel greening trend. *Geophysical Research Letters*, **32**, L21415.

Holben BN (1986) Characteristics of maximum-value composite images from temporal AVHRR data. *International Journal of Remote Sensing*, **7**, 1417–1434.

Huete AR, Huiqing L, Van Leeuwen WJD (1997) The use of vegetation indices in forested regions: issues of linearity and saturation. *Geoscience and Remote Sensing Symposium (IGARSS)*, **4**, 1966–1968.

Ichii K, Kawabata A, Yamaguchi Y (2002) Global correlation analysis for NDVI and climatic variables and NDVI trends: 1982–1990. *International Journal of Remote Sensing*, **23**, 3873–3878.

Jeyaseelan AT, Roy PS, Young SS (2007) Persistent changes in NDVI between 1982 and 2003 over India using AVHRR GIMMS (Global Inventory Modeling and Mapping Studies) data. *International Journal of Remote Sensing*, **28**, 4927–4946.

Julien Y, Sobrino JA, Verhoef W (2006) Changes in land surface temperatures and NDVI values over Europe between 1982 and 1999. *Remote Sensing of Environment*, **103**, 43–55.

Kaufmann RK, Zhou L, Knyazikhin Y, Shabanov V, Myneni RB, Tucker CJ (2000) Effect of orbital drift and sensor changes on the time series of AVHRR vegetation index data. *IEEE Transactions on Geoscience and Remote Sensing*, **38**, 2584–2597.

Kawabata A, Ichii K, Yamaguchi Y (2001) Global monitoring of interannual changes in vegetation activities using NDVI and its relationships to temperature and precipitation. *International Journal of Remote Sensing*, **22**, 1377–1382.

Koh LP, Miettinen J, Liew SC, Ghazoul J (2011) Remotely sensed evidence of tropical peatland conversion to oil palm. *Proceedings of the National Academy of Sciences*, **108**, 5127–5132.

Lark RM, Cullis BR, Welham SJ (2006) On spatial prediction of soil properties in the presence of a spatial trend: the empirical best linear unbiased predictor (E-BLUP) with REML. *European Journal of Soil Science*, **57**, 787–799.

Loveland TR, Belward AS (1997) The International Geosphere Biosphere Programme Data and Information System global land cover data set (DISCover). *Acta Astronautica*, **41**, 681–689.

Loveland TR, Reed BC, Brown JF, Ohlen DO, Zhu Z, Yang L, Merchant JW (2000) Development of a global land cover characteristics database and IGBP DISCover from 1 km AVHRR data. *International Journal of Remote Sensing*, **21**, 1303–1330.

Mann CC (2009) Addicted to Rubber. *Science*, **325**, 564–566.

Mitchell TD, Jones PD (2005) An improved method of constructing a database of monthly climate observations and associated high-resolution grids. *International Journal of Climatology*, **25**, 693–712.

Myneni RB, Hall FG, Sellers PJ, Marshak AL (1995) The interpretation of spectral vegetation indexes. *IEEE Transactions on Geoscience and Remote Sensing*, **33**, 481–486.

Nagol JR, Vermote EF, Prince SD (2009) Effects of atmospheric variation on AVHRR NDVI data. *Remote Sensing of Environment*, **113**, 392–397.

Nelson GC, Bennett E, Berhe AA *et al.* (2006) Anthropogenic drivers of ecosystem change: an overview. *Ecology & Society*, **11**, 29.

Nemani RR, Keeling CD, Hashimoto H *et al.* (2003) Climate-driven increases in global terrestrial net primary production from 1982 to 1999. *Science*, **300**, 1560–1563.

Nicholson S (2000) Land surface processes and Sahel climate. *Reviews of Geophysics*, **38**, 117–138.

Oliveira PJC, Davin EL, Levis S, Seneviratne SI (2011) Vegetation-mediated impacts of trends in global radiation on land hydrology: a global sensitivity study. *Global Change Biology*, **17**, 3453–3467.

Olsson L, Eklundh L, Ardö J (2005) A recent greening of the Sahel – trends, patterns and potential causes. *Journal of Arid Environments*, **63**, 556–566.

Pelkey NW, Stoner CJ, Caro TM (2000) Vegetation in Tanzania: assessing long term trends and effects of protection using satellite imagery. *Biological Conservation*, **94**, 297–309.

Pouliot D, Latifovic R, Olthof I (2009) Trends in vegetation NDVI from 1 km AVHRR data over Canada for the period 1985–2006. *International Journal of Remote Sensing*, **30**, 149–168.

Prince SD, Becker-Reshef I, Rishmawi K (2009) Detection and mapping of long-term land degradation using local net production scaling: application to Zimbabwe. *Remote Sensing of Environment*, **113**, 1046–1057.

Prishchepov AV, Radeloff VC, Baumann M, Kuemmerle T, Müller D (2012) Effects of institutional changes on land use: agricultural land abandonment during the transition from state-command to market-driven economies in post-Soviet Eastern Europe. *Environmental Research Letters*, **7**, 024021.

R Development Core Team (2012) *R: A Language and Environment for Statistical Computing*. R Foundation for Statistical Computing, Vienna, Austria. ISBN 3-900051-07-0. Available at: http://www.R-project.org/.

Roderick M, Farquhar G, Berry S, Noble I (2001) On the direct effect of clouds and atmospheric particles on the productivity and structure of vegetation. *Oecologia*, **129**, 21–30.

Roerink GJ, Menenti M, Verhoef W (2000) Reconstructing cloudfree NDVI composites using Fourier analysis of time series. *International Journal of Remote Sensing*, **21**, 1911–1917.

Running SW, Loveland TR, Pierce LL (1994) A vegetation classification logic based on remote sensing for use in global biogeochemical models. *Ambio*, **23**, 77–81.

Running SW, Nemani RR, Heinsch FA, Zhao M, Reeves M, Hashimoto H (2004) A continuous satellite-derived measure of global terrestrial primary production. *BioScience*, **54**, 547–560.

Seaquist JW, Hickler T, Eklundh L, Ardö J, Heumann BW (2008) Disentangling the effects of climate and people on Sahel vegetation dynamics. *Biogeosciences*, **6**, 469–477.

Slayback DA, Pinzon JE, Los SO, Tucker CJ (2003) Northern hemisphere photosynthetic trends 1982–99. *Global Change Biology*, **9**, 1–15.

Soja AJ, Cofer WR, Shugart HH, Sukhinin AI, Stackhouse PW Jr, Mcrae DJ, Conard SG (2004) Estimating fire emissions and disparities in boreal Siberia (1998–2002). *Journal of Geophysical Research*, **109**, D14S06.

Spitters CJT, HaJM T, Goudriaan J (1986) Separating the diffuse and direct component of global radiation and its implications for modeling canopy photosynthesis Part I. Components of incoming radiation. *Agricultural and Forest Meteorology*, **38**, 217–229.

Steinberg D (2009) CART: classification and regression trees. In: *The Top Ten Algorithms in Data Mining* (eds Wu X, Kumar V), pp. 179–201. CRC Press (Taylor & Francis Group), Boca Raton, FL.

Stöckli R, Vidale PL (2004) European plant phenology and climate as seen in a 20-year AVHRR land-surface parameter dataset. *International Journal of Remote Sensing*, **25**, 3303–3330.

Tucker CJ, Slayback DA, Pinzon JE, Los SO, Myneni RB, Taylor MG (2001) Higher northern latitude normalized difference vegetation index and growing season trends from 1982 to 1999. *International Journal of Biometeorology*, **45**, 184–190.

Tucker C, Pinzon J, Brown M *et al.* (2005) An extended AVHRR 8 km NDVI dataset compatible with MODIS and SPOT vegetation NDVI data. *International Journal of Remote Sensing*, **26**, 4485–4498.

Van Asselen S, Verburg PH (2012) A Land System representation for global assessments and land-use modeling. *Global Change Biology*, **18**, 3125–3148.

Verburg PH, Neumann K, Nol L (2011) Challenges in using land use and land cover data for global change studies. *Global Change Biology*, **17**, 974–989.

Viglizzo EF, Frank FC, Carreno LV *et al.* (2011) Ecological and environmental footprint of 50 years of agricultural expansion in Argentina. *Global Change Biology*, **17**, 959–973.

Wessels KJ, Prince SD, Malherbe J, Small J, Frost PE, Vanzyl D (2007) Can human-induced land degradation be distinguished from the effects of rainfall variability? A case study in South Africa. *Journal of Arid Environments*, **68**, 271–297.

Wessels KJ, Van Den Bergh F, Scholes RJ (2012) Limits to detectability of land degradation by trend analysis of vegetation index data. *Remote Sensing of Environment*, **125**, 10–22.

Wild M, Gilgen H, Roesch A *et al.* (2005) From Dimming to Brightening: decadal Changes in Solar Radiation at Earth's Surface. *Science*, **308**, 847–850.

Woodward FI, Lomas MR, Quaife T (2008) Global responses of terrestrial productivity to contemporary climatic oscillations. *Philosophical Transactions of the Royal Society B: Biological Sciences*, **363**, 2779–2785.

Xiao J, Moody A (2005) Geographical distribution of global greening trends and their climatic correlates: 1982–1998. *International Journal of Remote Sensing*, **26**, 2371–2390.

Zak MR, Cabido M, Cáceres D, Díaz S (2008) What drives accelerated land cover change in central Argentina? Synergistic Consequences of Climatic, Socioeconomic, and Technological Factors. *Environmental Management*, **42**, 181–189.

Zhang R, Delworth TL (2006) Impact of Atlantic multidecadal oscillations on India/Sahel rainfall and Atlantic hurricanes. *Geophysical Research Letters*, **33**, L17712.

Zhao M, Running SW (2010) Drought-induced reduction in global terrestrial net primary production from 2000 through 2009. *Science*, **329**, 940–943.

Zhao M, Running SW (2011) Response to comments on 'drought-induced reduction in global terrestrial net primary production from 2000 through 2009'. *Science*, **333**, 1093.

Zhou L, Tucker CJ, Kaufmann RK, Slayback DA, Shabanov NV, Myneni RB (2001) Variations in northern vegetation activity inferred from satellite data of vegetation index during 1981 to 1999. *Journal of Geophysical Research*, **106**, 20269–20283.

Zhuravleva TB, Rublev AN, Udalova TA, Chesnokova TY (2006) On calculation of photosynthetically active radiation in estimation of carbon balance parameters of surface ecosystems. *Atmospheric and Oceanic Optics*, **19**, 57–59.

Supporting Information

Additional Supporting Information may be found in the online version of this article:

Data S1. Supporting online material (SOM).
Figure S1. Maximum likelihood estimation of spatial model parameters.